Dynamic Analysis of a Curved Floating Bridge

Analyse dynamique d'un pont courbe flottant

Dynamische Berechnung einer gekrümmten schwimmenden Brücke

I. HOLAND

Professor, dr. techn.
Norwegian Institute of Technology
Trondheim, Norway

R. SIGBJÖRNSSON

Research Engineer, lic. techn.
SINTEF
Trondheim, Norway

I. LANGEN

Research Engineer
SINTEF
Trondheim, Norway

SUMMARY

A curved floating bridge subjected to wave loading is analyzed. The structural model is made up of straight beam elements, and the hydrodynamic model is based on the two-dimensional potential theory. Results of forced deterministic vibration analyses are given for three sinusoidal wave patterns. The response to irregular waves is investigated in the time domain by a Monte Carlo technique. A sea state described by the JONSWAP spectrum is simulated, and expected peak response and standard deviations are found by a statistical treatment of the time series.

RÉSUMÉ

Un pont courbe flottant est soumis à l'action des vagues. Le modèle statique se compose d'éléments de poutres rectilignes. Le modèle hydrodynamique est basé sur la théorie des potentiels, à deux dimensions. Les résultats de l'analyse des vibrations de type déterministique forcé sont présentés pour trois cas de houle de forme sinusoïdale. L'effet, dans le temps, de vagues irrégulières est étudié au moyen de la technique de Monte Carlo. Des conditions maritimes sont simulées selon le spectre JONSWAP et les valeurs extrêmes et déviations standard sont obtenues par traitement statistique de séries dans le temps.

ZUSAMMENFASSUNG

Eine von Wellen beanspruchte, gekrümmte schwimmende Brücke wird berechnet. Das statische Modell ist aus geraden Balkenelementen zusammengesetzt. Dem hydrodynamischen Modell liegt eine zwei-dimensionale Potentialtheorie zu Grunde. Resultate von gezwungenen deterministischen Schwingungsberechnungen werden für drei sinusförmige Wellen gegeben. Die Reaktion auf irreguläre Wellen wird als Zeitfunktion mit einer Monte Carlo-Technik untersucht. Ein Wellenzustand nach dem JONSWAP-Spectrum wird simuliert, und erwartete Extremwerte und Standardabweichungen werden mittels einer statistischen Behandlung der Zeitreihen gefunden.

THE SALHUS BRIDGE PROJECT

The Norwegian Public Roads Administration considers a floating bridge or a sus-
pension bridge to replace the ferry connection across the Salhus Fiord north of
Bergen.

The floating bridge, that shall be discussed here, is designed as a horizontal
arch, see Fig. 1. The traffic runs on a concrete slab supported by columns from
a continuous pontoon, see Fig. 2. The bridge is designed with the minimum
dimensions given in Fig. 2, except at the southern end. Here the slab has been
raised to allow sufficient free sailing space, see Fig. 1. The number of cells
(three in Fig. 2) is supposed to be increased to maximum 7 at the southern end.

To allow the bridge to follow the tide variation, hinge sections are provided
at the ends, see Fig. 3.

The governing loading originates from the waves. Thus a dynamic analysis is
mandatory. The Division of Structural Mechanics and the Engineering Research
Foundation at the Norwegian Institute of Technology have been engaged to carry
out these analyses, which have been reported in [1] through [6]. The main
features and results shall be described here. The project is still under evalu-
ation, and possible redesigns to improve the dynamic behaviour are being con-
sidered.

THE STRUCTURAL MODEL

The curved bridge was modelled by 20 straight beam elements (see Fig. 1), each
61.72 m long and with uniform cross section. In the part with variable cross-
section, the midpoint of the element was chosen to be representative.

The standard equation of motion may be written

$$K r + C \dot{r} + M \ddot{r} = R(t) \tag{1}$$

in which

K	= stiffness matrix,	M	= mass matrix,
r	= vector of nodal displacement parameters,	$R(t)$	= vector of external forces,
		t	= time, and
C	= damping matrix,	$\cdot$	= time derivative.

In the displacement vector r the three translational and the three rotational
components at each node were included. The load vector $R(t)$ contains the
corresponding load.

The stiffness matrix K was based on the traditional beam bending theory, ex-
cluding shear strain, and on the St.Venant theory of torsion. Axial strain was
included. The contribution from the bridge deck to the stiffness of the cross-
section was neglected because of large flexibility of the columns in comparison
with the box-shaped pontoon. Therefore only the cross-section of the pontoon
was considered to take axial forces and bending and torsional moments, and the
motion of the bridge was related to the centre of shear D of the pontoon alone
(see Fig. 2). Additional terms were added to the stiffness matrix for vertical
and torsional motion, to take into account the buoyancy effect.

The mass M is the sum of a structural mass matrix and a hydrodynamic mass matrix.
The whole cross-section was considered for mass calculation, and thus the centre
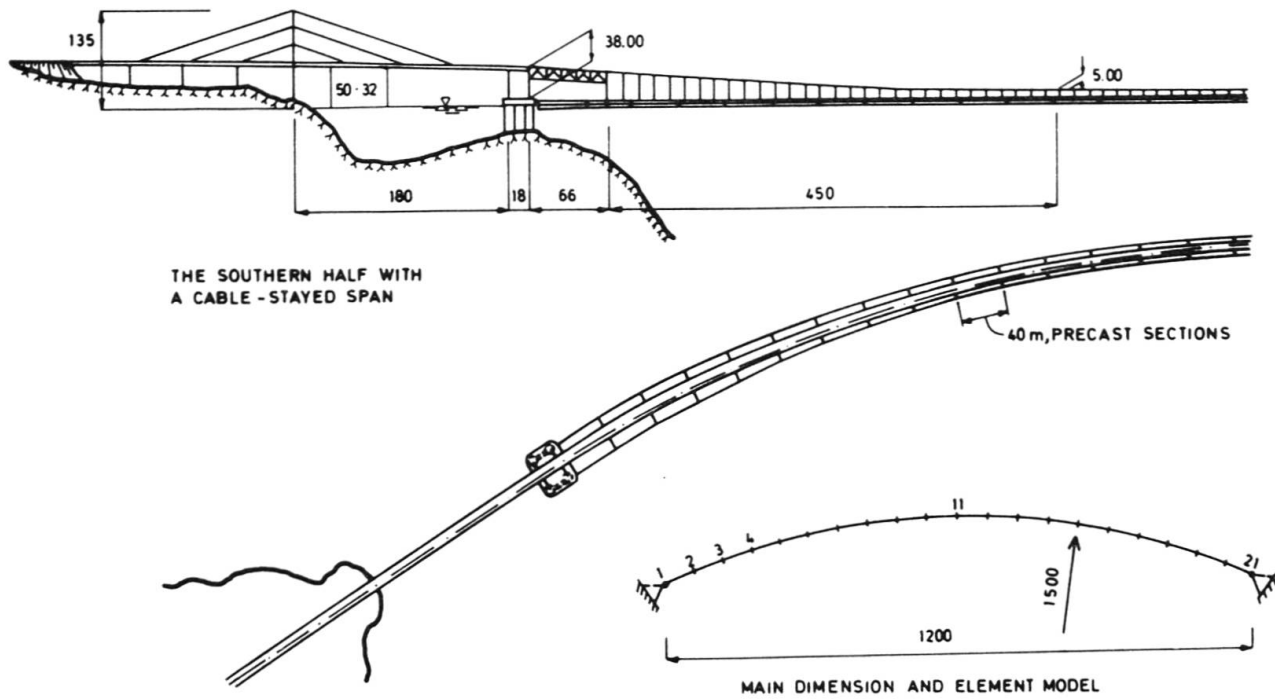
THE SOUTHERN HALF WITH
A CABLE-STAYED SPAN

40 m, PRECAST SECTIONS

MAIN DIMENSION AND ELEMENT MODEL

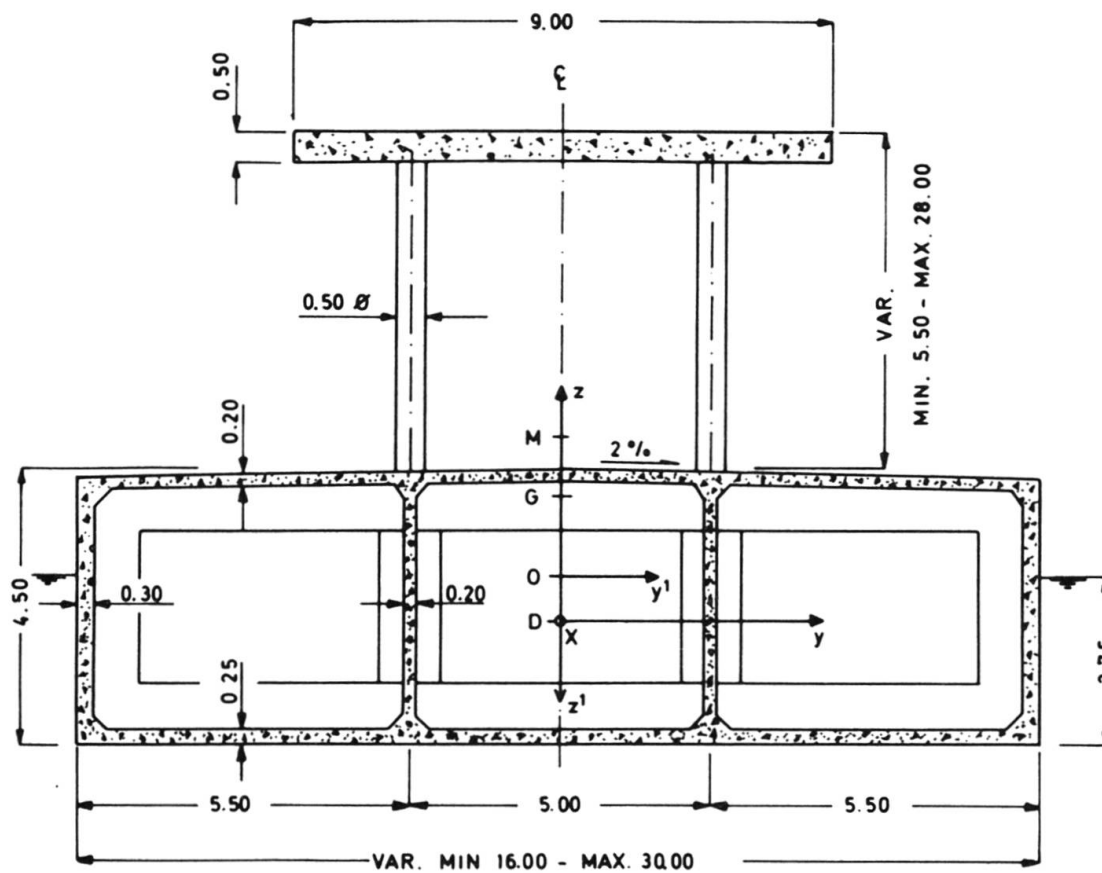FIGURE 1   THE SALHUS FLOATING BRIDGE.   DIMENSIONS IN m

FIGURE 2   CROSS-SECTION.   DIMENSIONS IN m

of gravity G was located above the centre of shear D.

The damping in the structure is considered to be small compared with the hydro-
dynamic damping. Therefore only hydrodynamic terms were included in the damping
matrix C, which is not orthogonal with respect to the natural modes.

The buoyancy forces, the inertia forces and the damping forces were assumed to
be distributed along the bridge, and the corresponding matrices were consistent
with the assumed displacement field for the beam element.

The hinge structures at the end were simulated by the boundary conditions shown
in Fig. 3.

FIGURE 3   HINGE SECTION AND
           BOUNDARY CONDITIONS
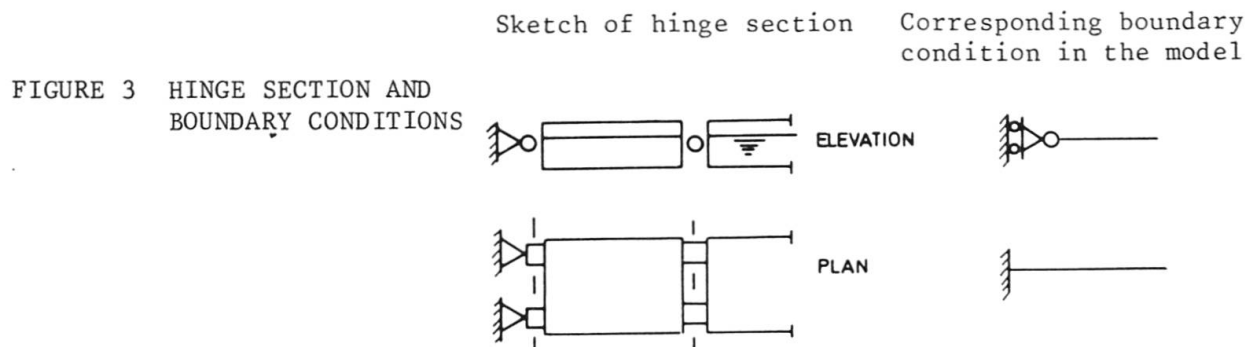
Eq. (1) was solved by direct numerical integration using "the constant average
acceleration method", which is also known as the Newmark method with $\beta = 1/4$.

The general finite element program used in the dynamic analysis is a modified
version of the computer program FEDA [3,7].

THE HYDRODYNAMIC MODEL

The water pressure on the pontoon induced by the motion of the pontoon itself
and the waves may be interpreted as a set of hydrodynamic mass, damping and
restoring buoyancy forces, and wave forces. The calculation of these forces is
herein based on three main assumptions: (1) linearity, (2) two-dimensional flow,
(3) potential flow.

Re. 1: A linear hydrodynamic model is used. This assumption implies that the
principle of superposition holds, that hydrodynamic damping and hydrodynamic
mass may be found assuming the pontoon acting like a wave generator in calm
water, that wave forces are equivalent to those due to wave action on a re-
strained pontoon, and that influence from the wavy surface is neglected when
calculating restoring buoyancy forces.

Re. 2: The evaluation of the hydrodynamic forces is based on two-dimensional
theory and experiments. This assumption is reasonably well satisfied when the
ratio between the width of the pontoon and the distance between two adjacent
nodes in the actual mode of vibration is small. This ratio is in the present
case about 1/10 for the modes in question. For the wave forces this implies
that they are related to a situation where the wave crests are tangential to
the bridge arch.

Re. 3: The whole hydrodynamic problem is solved inside the framework of the
potential theory. Hence, the velocity potential is obtained by solving the two-
dimensional Laplace equation with the relevant initial and linearized boundary
conditions.

According to [8,9], these conditions are approximately fulfilled in many problems
associated with ship motions, with some reservations for viscous effects, with
increased damping in sway and roll. As all motion, in particular roll, is small
for the actual bridge in comparison with a ship, the assumptions above should be
satisfied with a reasonable degree of accuracy.

Let $Oy'z'$ be a coordinate system which is fixed in space as shown in Fig. 2.
The y'-axis is placed in the water surface, and the z'-axis is vertical, positive
downwards. The origin 0 is the intersection of the centreline of the section and
the waterline. The body is assumed symmetric about the z-axis. In this co-
ordinate system the forces per unit length of the pontoon may be expressed for
sway as [8]

$$Y' = -a_{yy}\ddot{y}' - b_{yy}\dot{y}' - a_{y\phi}\ddot{\phi}' - b_{y\phi}\dot{\phi} + Y'_w \qquad (2)$$

where

ϕ' = rotation in the $y'-z'$- $\quad a_{y\phi}=a_{\phi y}$ = coupling masses,
plane, about 0, $\quad b_{y\phi}=b_{\phi y}$ = coupling damping, and

a_{yy} = hydrodynamic mass, $\quad Y'_w$ = wave force.

b_{yy} = hydrodynamic damping,

According to the model all these quantities depend on frequency.

Referring back to Eq. (1), the a-terms of Eq. (2) enter the mass matrix M, the
b-terms the damping matrix C and the force components Y'_w the load vector $R(t)$.

The sway component of the exciting force induced by a sinusoidal wave with a unit
amplitude
$$\zeta = \sin\omega t \qquad (3)$$

may be expressed as

$$Y'_w = Y'_a \sin(\omega t - \varepsilon_{y\zeta}) \qquad (4)$$

where Y'_a is a frequency dependent amplitude, and $\varepsilon_{y\zeta}$ a frequency dependent phase
angle referred to wave elevation at 0 (see Fig. 2).

The heave and roll forces are governed by equations similar to Eqs. (2) and (4).
These equations show that the sway and roll forces are coupled.

In the structural analysis the reponse is best referred to the centre of shear
D (see Fig. 2). Therefore Eq. (2) is transformed to the Dyz-coordinate system
shown in Fig. 2 before substitution into Eq. (1).

Frank [10] and Vugts [8,9] have calculated the wave force amplitudes and the
hydrodynamic quantities for heave and roll for different types of ship-like
sections using different numerical schemes. Faltinsen [11] has compared the
methods for rectangular sections. The results show good agreement.

Vugts [8,9] has also compared his theoretical results with experimental results
over a large range of frequencies. For the Salhus bridge project two-dimensional
experiments with a rectangular pontoon were carried out for a limited number

of frequencies [13]. Comparisons show that all the hydrodynamic quantities can be computed with sufficient accuracy by potential theory. One important exception is the roll damping, where the viscous effects are much more important than in heave and sway.

The hydrodynamic quantities applied in the present study were mainly derived from the results given by Vugts [8,9].

In the case of stationary forced vibration the hydrodynamic quantities were evaluated for the wave period, and in the case of random vibration for the peak period of the wave spectrum, while in the case of natural vibration an iteration loop was devised to adjust the hydrodynamic quantities to the actual natural period.

NATURAL VIBRATIONS

The analysis of natural vibration is a prerequisite for more exhaustive dynamic analyses, but it does also provide considerable insight in the dynamic characteristics of the structure.

The natural modes and periods resulting from the finite element analysis are shown in Fig. 4 for modes 1 through 7 and mode 13. Modes 1 and 3 are sway modes (horizontal motion), modes 2, and 5 through 7, are heave modes (vertical motion), and mode 13 is a combined roll-sway mode. Modes 8 through 12, that are not shown, are all heave modes with an increasing number of nodes of vibration.

The heave periods show only small differences. This is a result of the dominance of the buoyancy in the stiffness matrix. The natural period T for vertical rigid body motion of a floating beam or arch is given by the traditional formula

$$T = 2\pi\sqrt{m/k} \tag{5}$$

where m and k are mass and restoring buoyancy force per unit length, respectively. Consider next a floating arch, idealized as a line rotating rigidly a small angle θ about an axis of gravity $y = 0$ (see Fig. 5). The undamped motion is governed by

$$\theta\int_s my^2 ds + \theta\int_s ky^2 ds = 0 \tag{6}$$

where s is a coordinate measured along the arch. If m and k are constant along the arch, the natural period in rigid body rotation will equal that for heave. The same applies to rotation about the y-axis. Thus, an idealized arch has three identical natural periods, for vertical motion and for rotation about two horizontal axes. The finite width of the arch causes only a slight disturbance of this conclusion.

Natural periods decrease only slightly when modes of vibration that include moderate straining from bending and torsion are considered. This is easily demonstrated for the case of a floating straight beam with simply supported ends. The mode shapes will be sinusoidal, and the natural period is found to be

$$T = 2\pi\sqrt{m/(k+EI(\frac{n\pi}{\ell})^4)} \tag{7}$$

where
EI = bending stiffness of the beam,
ℓ = beam length, and
n = number of half waves.

NO. 1
T = 11 s

NO. 2
T = 6.8 s

NO. 3
T = 6.6 s

NO. 4
T = 6.26 s

NO. 5
T = 5.857 s

NO. 6
T = 5.851 s

NO. 7
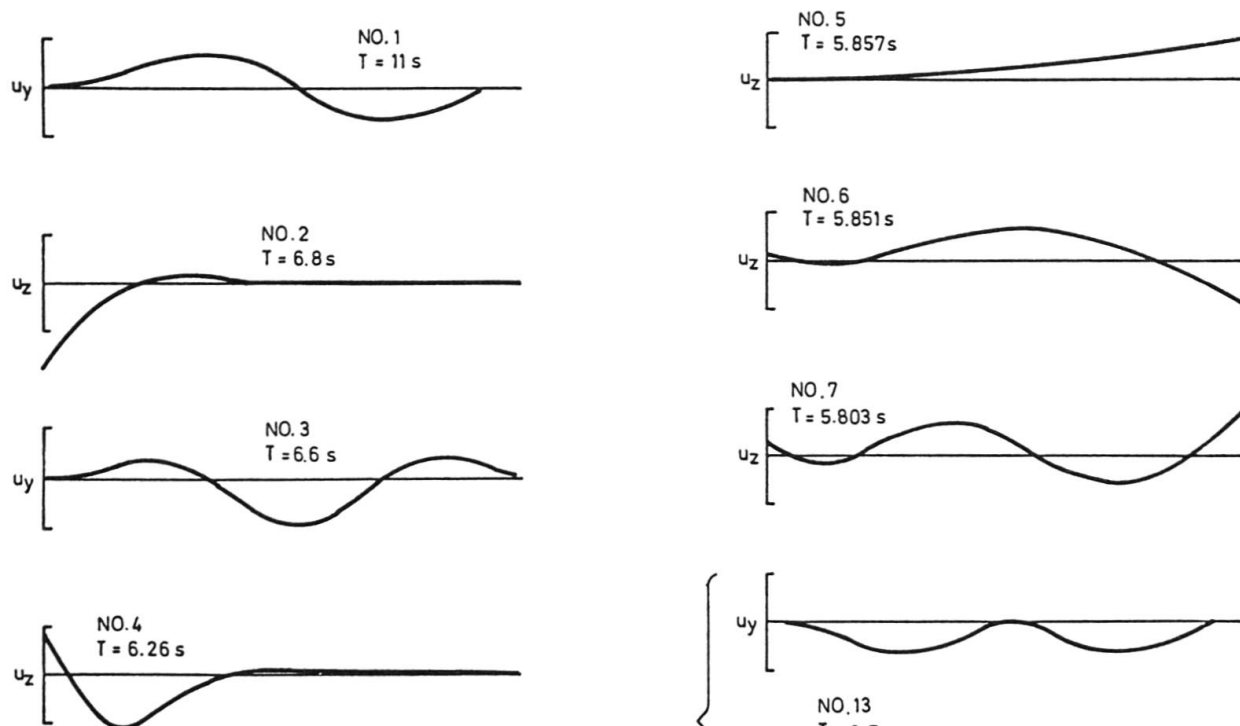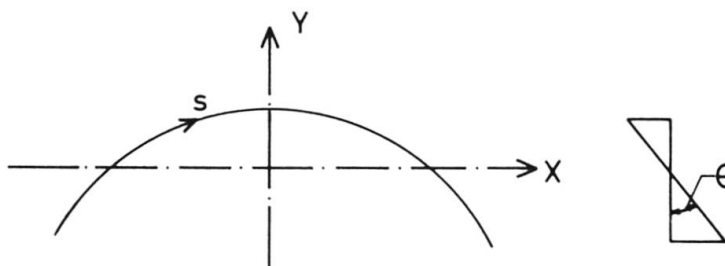T = 5.803 s

NO. 13
T = 3.7 s

FIGURE 4   NATURAL MODES OF VIBRATION

u_y radial displacement

u_z vertical displacement

ϕ_x rotation about the bridge axis

FIGURE 5   LINE IDEALIZATION AND
ROTATION OF AN ARCH

For beams of the length considered here, the bending stiffness term in the paranthesis in Eq. (7) is secondary, and Eq. (7) will give a natural frequency only slightly different from Eq. (5) for moderate values of n.

The conclusion is that there will be a narrow band of natural periods close to the rigid body period for heave, corresponding to a variety of mode shapes. This fact implies that the bridge is particularly exposed to excitation from wave spectra with peak frequencies close to the rigid body heave frequency. Furthermore, for a structure with a certain mass per unit length, this band of natural frequencies can only be shifted by a change of the water surface area.

The natural periods predicted above are confirmed by the numerical results. Data for maximum m and k give, by using Eq. (5),

$$T = 7.03 \text{ s, to be compared to } T_2 = 6.8 \text{ s}$$

T_2 corresponds to heave motion of the end with maximum dimensions. The mode includes considerable bending and also motion of sections with smaller dimensions (see Fig. 4, No. 2). Hence, a reduction of the period for pure rigid body motion of the largest section results.

Data for minimum m and k give, by using Eq. (5)

$$T = 5.857 \text{ s to be compared with } T_5 = 5.857 \text{ s}$$

The mode shape (see Fig. 4, No. 5) corresponds to a nearly rigid motion of the bridge, where the enlarged southern part is at rest.

Modes 6 and 7 confirm the minor influence of bending predicted by Eq. (7).

Natural modes in roll are coupled with those in heave because of the curvature of the bridge. Only in the case of a straight symmetric beam complete uncoupling occurs. Natural modes in sway are coupled with those in roll partly due to coupling in hydrodynamic sway and roll forces and partly because the centre of gravity does not coincide with the shear centre.

Numerical results show, however, that coupling is insignificant for this structure in most cases. Thus coupling is on the noise level and not shown for all vibrations up to and including No. 12.

FORCED DETERMINISTIC VIBRATIONS

Three cases of response due to regular wave patterns are shown in Table 1. Long-crested waves with two different directions, based on observations and topography, were selected (cases 1 and 2). In addition, "short-crested" waves at the bridge centre were included (case 3).
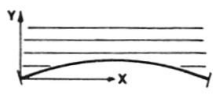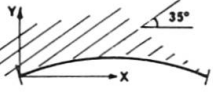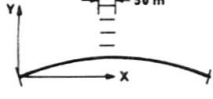
The wave period was chosen

$$T = 5.8 \text{ s}$$

close to a number of resonance periods in heave, in order to excite resonant heave motion. This period is also fairly close to the resonant sway period for mode No. 3 (see Fig. 4). The wave length determines the phase lag between forces in different nodal points. It was chosen as 52.5 m in accordance with the Airy wave theory for deep water, and the wave heights were chosen equal to 2 m (peak to peak).

The results were obtained as functions of time and location, and showed that a multitude of natural modes were excited (see [5]). Only the maximum displacement values are included in Table 1. They are located at the middle of the bridge for the cases 1 and 3, and at the southern end (x=y=0) for case 2. The largest response is induced for load case 1. The reason is that the wave load near the middle of the bridge is almost in phase over a width of, say, 300 m. An important result is that the vertical motion exceeds the wave heights by 50 per cent.

In load case No. 2 only heave motion of the southern part of the bridge is significant, and the forced mode is essentially a combination of the natural

TABLE 1   Steady state vibra-
tions of the bridge
subjected to sinus-
oidal wave loading.
Load shapes and
maximum displacements
observed. Single
wave amplitude equal
to 1 m

Case No.	Shape	Period (s)	u_x (m)	u_y (m)	u_z (m)	ϕ_x (rad)
1		5.8	0.12	1.52	1.50	0.0050
2		5.8	$\simeq 0$	0.01	0.82	0.0004
3		5.8	0.02	0.25	0.25	0.0007

modes Nos. 2 and 4. This result indicates that a forced period of, say 6.8 s,
would have induced an appreciably larger heave response for load case 2.

Internal stress resultants obtained simultaneously from the finite element
analysis are omitted here, see [5].

RANDOM VIBRATIONS

The basic assumption in this analysis is that the surface elevation of the sea
can be approximated as an ergodic Gaussian process. It is felt that this assump-
tion is reasonable in an engineering analysis both from a theoretical (the cen-
tral limit theorem) and an experimental point of view (see [14]).

A basic representation of an ergodic Gaussian process $\{\zeta(t); -\infty < t < \infty\}$, with zero
mean and a power spectral density $S_\zeta(\omega)$, $0 < \omega < \infty$, is given by [15,16,17]

$$\zeta(t) = \sigma_\zeta \sqrt{\frac{2}{N}} \sum_{i=1}^{N} \cos(\omega_i t - \phi_i) \qquad (8)$$

Here ϕ_i, $i = 1,2, \ldots, N$, are independent random phase angles distributed uni-
formly between 0 and 2π and ω_i, $i = 1,2 \ldots, N$, are realizations of random fre-
quencies distributed according to the distribution function

$$F(\omega) = \sigma_\zeta^{-2} \int_0^\omega S_\zeta(u)du \qquad (9)$$

where σ_ζ denotes the standard deviation of wave elevation.

It is seen that $\zeta(t)$ as determined by Eq. (8) tends to be Gaussian by virtue of
the central limit theorem. It can be shown that $\zeta(t)$ is ergodic at least up to
the second moment. Furthermore, it can be shown that the spectral density of
$\zeta(t)$ converges to the tangent spectral density $S_\zeta(\omega)$ in the form $1/N^2$ as N
approaches infinity.

The results of the analysis of wave records indicate that the one-dimensional
wave spectral density in the Salhus Fiord is more narrow and more peaked than
wave spectral densities in open sea [18]. The JONSWAP spectral density

$$S_\zeta(\omega) = \alpha g^2 \omega^{-5} \exp\{-\tfrac{5}{4}(\tfrac{\omega}{\omega_p})^{-4}\}\gamma^{\exp\{-\frac{(1-\omega/\omega_p)^2}{\sigma}\}}$$ (10)

furnishes the desirable features [19].

Here

α = Phillips' parameter,   γ = peakedness parameter, and
g = acceleration of gravity, σ = parameter defining the width
ω_p = peak frequency,   of the spectral peak.

In this study ω_p is taken equal to 1.0833 rad/s, which corresponds to the period 5.8 s used in the deterministic analysis. The parameter σ is taken as

$$\sigma = 0.07 \quad \text{if} \quad \omega \leq \omega_p \quad \text{and} \quad \sigma = 0.09 \quad \text{if} \quad \omega > \omega_p$$

The peakedness parameter γ is taken equal to 7.0, which corresponds to a very sharply peaked spectrum. The Phillips' parameter α is adjusted so that the significant wave height is equal to 1 m, which gives α = 0.002. A reasonable estimate of the expected highest wave in a record is then approximately 2 m [6,18]. These parameters make it possible to compare the results from the present study with the results from the deterministic approach.

Heuristically, the sway forces induced by irregular waves simulated by Eq. (8) (see also Eq. (4)) can be expressed as

$$Y(t) = \sigma_\zeta \sqrt{\frac{2}{N}} \sum_{i=1}^{N} Y'_a(\omega_i)\cos(\omega_i t - \phi_i - \varepsilon_{y\zeta}(\omega_i))$$ (11)

This equation combined with Eqs. (9) and (10) provides a straight forward procedure to simulate the sway forces. The heave and roll forces can be obtained by a similar procedure.

Since the wave spectrum is narrow banded, wave force amplitudes and phase lags can with fair approximation be computed for the peak frequency.

The response can now be obtained by a numerical integration of the equations of motion Eq. (1), when the bridge is subjected to stationary irregular longcrested waves corresponding to load case No. 1 in Table 1. The length of the simulated wave situation was selected 500 seconds. The number of frequencies N used in the construction of the wave profile was taken equal to 999.

The results of the simulation are plotted in Fig. 6. The figure shows both the wave profile and the structural response, i.e. axial deflection, sway, heave and roll, as computed for the midpoint of the bridge.

The significant height calculated from the simulated wave situation is 0.95 m or 5 per cent less than the target significant wave height given by the spectral density. The empirical probability functions for the wave amplitudes are plotted in Fig. 7 together with the theoretical probability density functions. It is seen that the initial distribution follows the normal distribution, while the distribution of maxima and minima ζ_0 is represented fairly well by the following distribution [20]

$$p(\chi) = \frac{1}{\sqrt{2\pi}}[\varepsilon\exp\{-\tfrac{1}{2}\chi^2/\varepsilon^2\} + \sqrt{1-\varepsilon^2}\ \chi\exp\{-\tfrac{1}{2}\chi^2\}\int_{-\infty}^{\chi\sqrt{1-\varepsilon^2}/\varepsilon}\exp\{-\tfrac{1}{2}t^2\}dt]$$ (12)
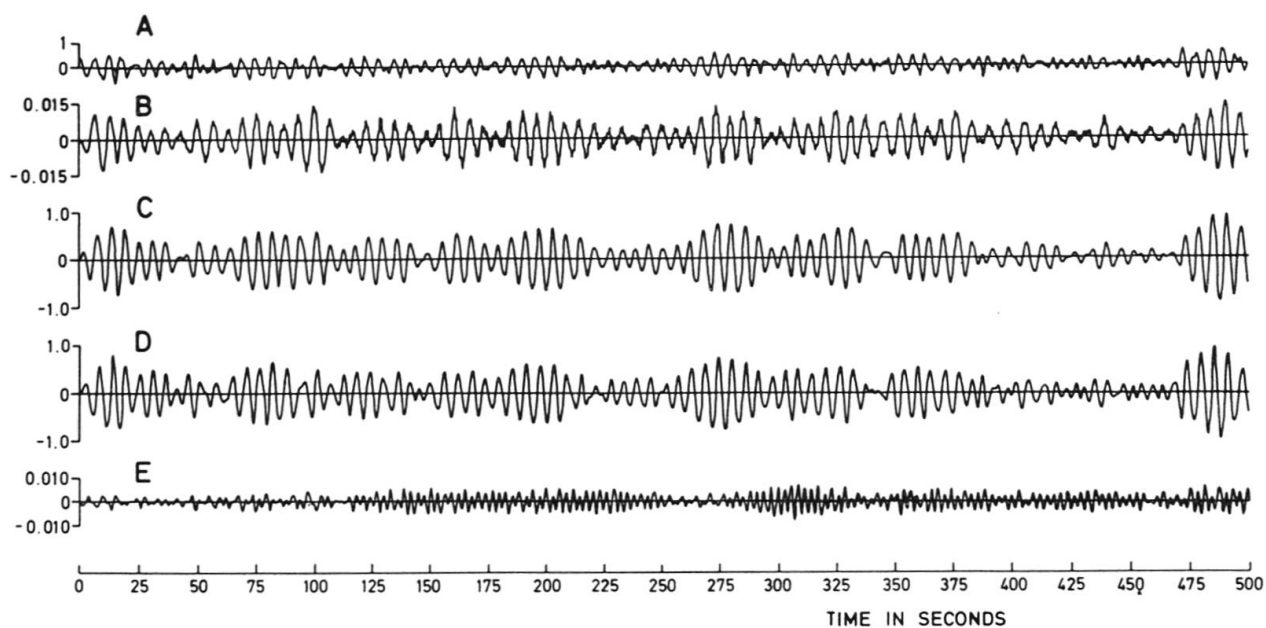
FIGURE 6   THE TIME HISTORIES OF WAVES AND STRUCTURAL RESPONSE
           (A) WAVE PROFILE, (B) AXIAL DEFLECTION, (C) SWAY,
           (D) HEAVE AND (E) ROLL

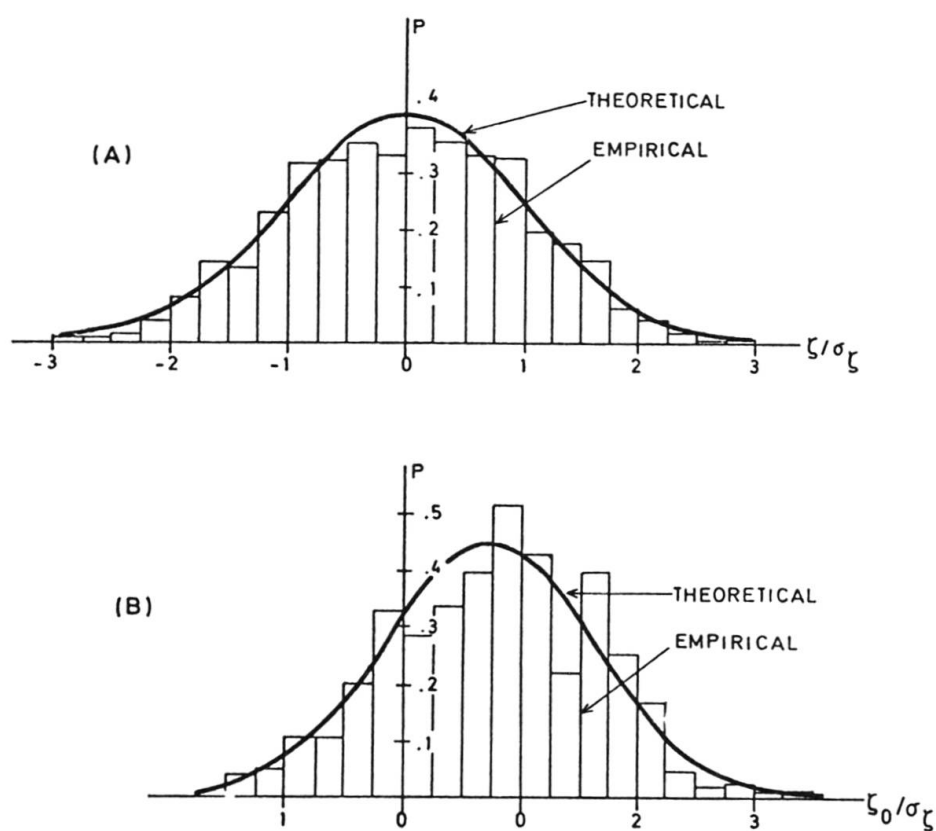

FIGURE 7   THE PROBABILITY DENSITY FUNCTIONS OF WAVE AMPLITUDES:
           (A) ALL AMPLITUDES ζ, σ_ζ = 0.2375 m; (B) MAXIMA AND MINIMA ζ_o,
           NUMBER OF MAXIMA m = 189, BANDWIDTH PARAMETER ε = 0.7940

where $\chi = \zeta_0/\sigma_\zeta$ and ϵ is the bandwidth parameter, which can be expressed in terms of the moments of the distribution. The bandwidth parameter was estimated to 0.7949, which is in agreement with the values derived from the wave measurements in [18]. Fig. 8 gives an example of the probability density function of the response.

It can be shown [20] by applying Eq. (16) that the expected largest maximum out of m independent maxima ζ_0 is given by

$$E[\zeta_{max}] = \sigma_\zeta \left[\sqrt{2\ln(m\sqrt{1-\epsilon^2})} + \frac{0.5772}{\sqrt{2\ln(m\sqrt{1-\epsilon^2})}} \right] \qquad (13)$$

The standard deviation of the largest maximum is given by

$$\sigma[\zeta_{max}] = \sigma_\zeta \frac{\pi}{\sqrt{6}} \frac{1}{\sqrt{2\ln(m\sqrt{1-\epsilon^2})}} \qquad (14)$$

The largest maximum and smallest minimum wave amplitude observed during the simulation is 0.67 and −0.77 m, respectively. The theoretical prediction of largest expected maximum (or minimum) is 0.77 m with a standard deviation equal to 0.10 m. This indicates that the simulated wave heights are acceptable.
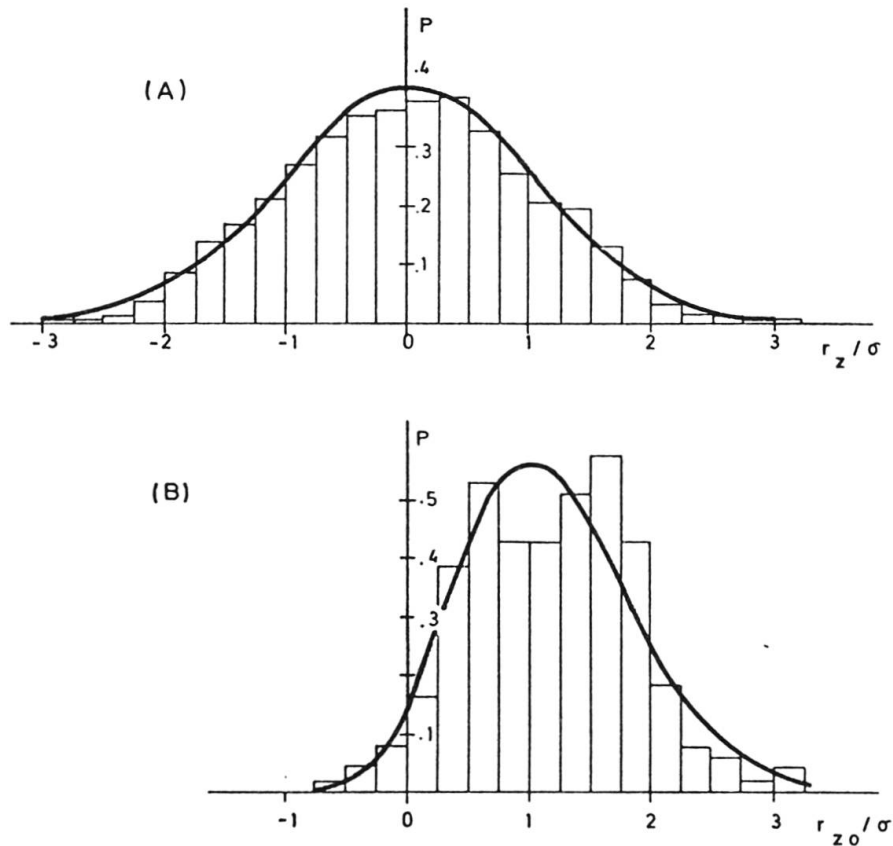

FIGURE 8   THE PROBABILITY DENSITY FUNCTIONS OF HEAVE MOTION AT THE MIDPOINT OF THE BRIDGE: (A) ALL AMPLITUDES, $\sigma = 0.3135$ m; (B) MAXIMA AND MINIMA, $m = 98$, $\epsilon = 0.3624$

TABLE 2   The largest observed response in the simulation compared with the
          expected largest response

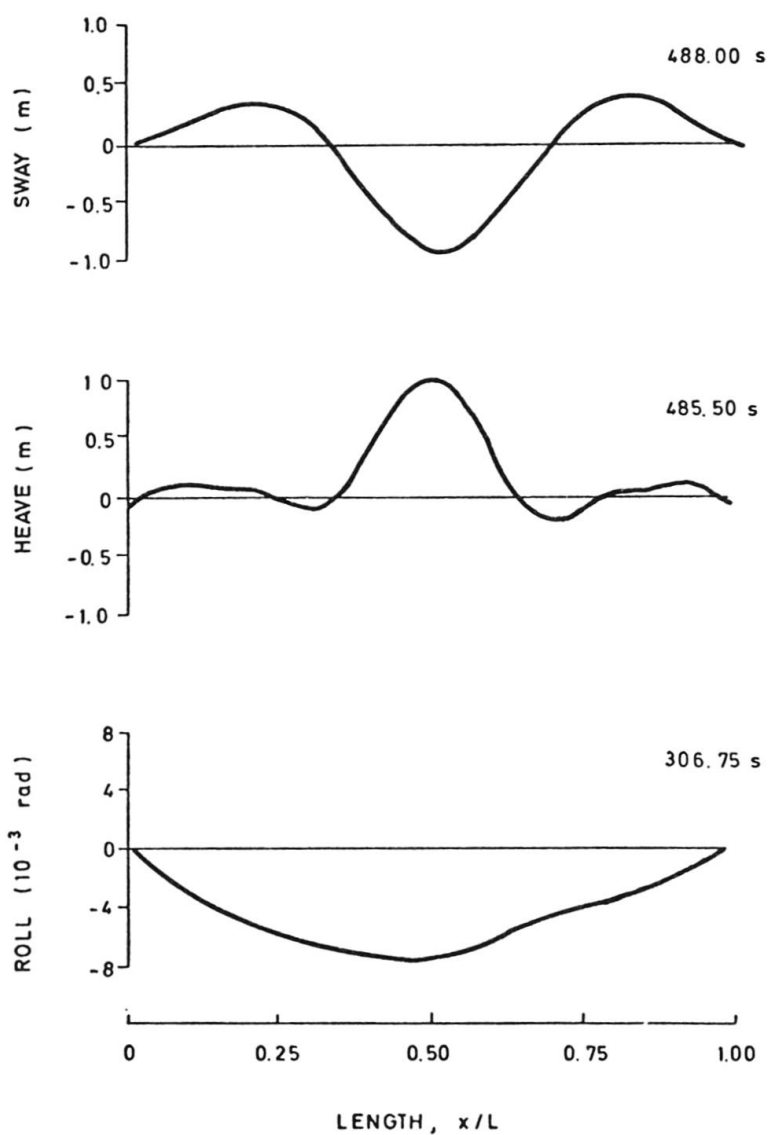| Response | Standard deviation | Largest observed | | Theoretical | |
		maximum	minimum	$E[r_{max}]$	$\sigma[r_{max}]$
Axial def. (m)	0.005	0.015	−0.014	0.017	0.002
Sway (m)	0.31	0.90	−0.92	1.00	0.13
Heave (m)	0.31	0.98	−0.95	1.00	0.13
Roll (m)	0.0026	0.0069	−0.0077	0.0089	0.0011

FIGURE 9   THE MODES OF VIBRATION SHOWING THE MAXIMUM RESPONSE OBSERVED
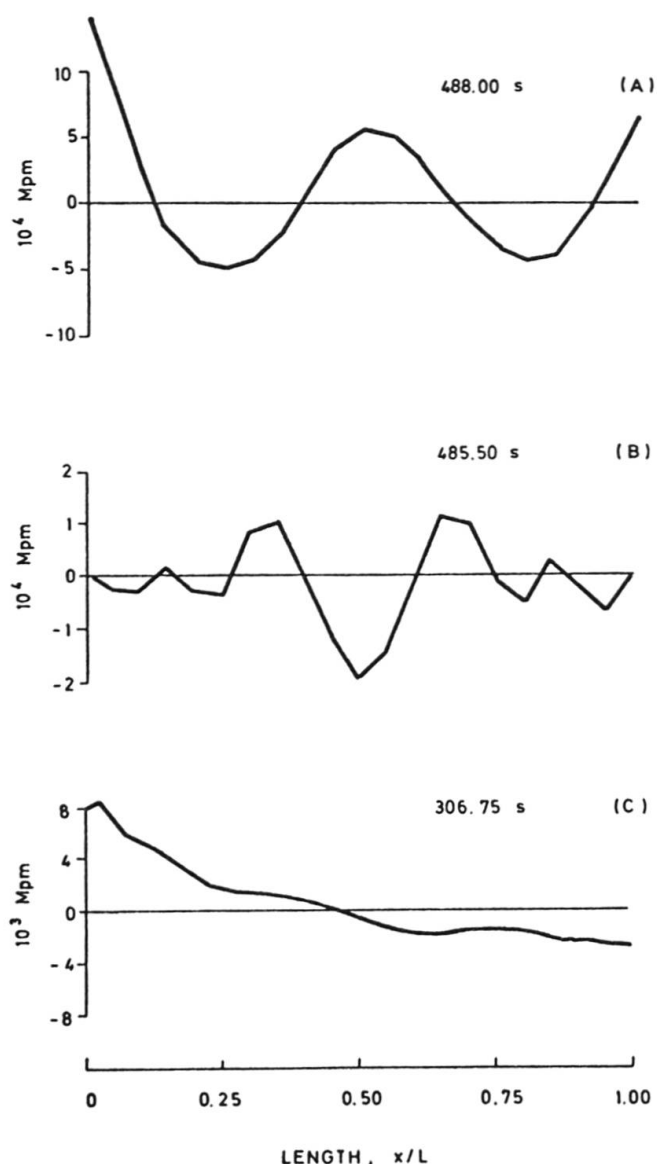
FIGURE 10   THE MAXIMUM RESPONSE OBSERVED:
            (A) bending moment about the local
                z-axis
            (B) bending moment about the local
                y-axis
            (C) twisting moment about the local
                x-axis

TABLE 3   Comparison of the response induced by
          irregular and regular waves

Response	Standard deviation	$E[r_{max}]$	r_{max} [1]
Axial def. (m)	0.006	0.022	0.12
Sway (m)	0.33	1.30	1.52
Heave (m)	0.33	1.30	1.50
Roll (rad)	0.0028	0.0113	0.0050

[1] Response induced by sinusoidal waves

In Table 2 the simulated peak response is compared with the expected largest response. The agreement is found satisfactory. The deviation between the observed and the theoretical values for sway and heave may be due to the fact that the maxima are not independent, but appear in clusters (see Fig. 6). The modes of vibration are plotted in Fig. 9 showing the same over- all characteristics as seen in the deterministic analysis. The maximum moments observed during the simulation are plotted in Fig. 10.

In the deterministic analysis the response was calculated for a sinusoidal wave with the wave height equal to 2 meters. Comparison of those results to the present results can be ob- tained by extrapolation, assum- ing the time series long enough to yield the expected largest wave amplitude equal to 1 m. The extrapolated response values are given in Table 3.

It is seen that the irregular waves induce somewhat smaller response than the sinusoidal waves, as expected. The only exception is the roll motion, which is larger in the irregu- lar case. This is mainly due to the fact that the irregular wave situation includes some higher frequency components which correspond to natural modes including roll, the first of which has a period of 3.7 s (see Fig. 4, No. 13). The reasons why the reduction in the response is not larger, are first of all rather high regu- larity in the irregular wave situation and rather large amount of damping.

CONCLUSION

Although analyses of natural vibrations and of motion in regular waves can provide considerable insight in the dynamic characteristics of the present structure, random vibration analysis appears to be the most rational means of providing response data applicable in design.

The stresses and displacements obtained by the analysis accomplished so far are hardly tolerable. However, recent observations [18] have shown a peak period in the wave spectrum of about 4 s. A change of the peak period from the applied resonant period of 5.8 s to 4 s will cause a considerable reduction in heave response and possibly also in sway response. An increase in roll response may, however, be foreseen. Therefore, the net result rests on a complete reanalysis.

If the proposed design finally proves inadequate after a realistic analysis, possibilities for improving the shape of the cross section exist. Such changes should have two aims; to increase the natural heave periods and to improve the hydrodynamic properties. This improvement should aim at a reduction of wave forces and an increase of hydrodynamic damping.

The numerical results reveal that in spite of non-uniform cross-section and several couplings in hydrodynamic and mechanical quantities, the dynamic characteristics of the floating arch bridge are rather simple. Thus, the coupling between different components of motion in the natural modes is weak, and natural frequencies can be predicted with a high degree of accuracy by simple formulas. This simplicity indicates that a far-going closed form stochastic analysis may be possible and should be explored further.

REFERENCES

1. Dynamiske beregninger av flytebro over Salhusfjorden, Division of Structural Mechanics, The Technical University of Norway, Trondheim, Jan. 1970.

2. HOLAND, I. and LANGEN, I.: Salhus floating bridge: Theory and hydrodynamic coefficients, SINTEF Report, Nov. 15th, 1972.

3. HOLAND, I. and LANGEN, I.: Salhus floating bridge: Dynamic analyses for regular wave pattern, SINTEF Report, Nov. 20th, 1972.

4. HOLAND, I. and LANGEN, I.: Salhus floating bridge: Dynamic analysis with new boundary conditions, SINTEF Report, Dec. 19th, 1972.

5. SIGBJÖRNSSON, R. and LANGEN, I.: Wave-induced vibrations of a floating bridge: The Salhus Bridge, SINTEF Report STF 71 A75018, 1975.

6. SIGBJÖRNSSON, R. and LANGEN, I.: Wave-induced vibrations of a floating bridge: A Monte Carlo Approach, SINTEF Report STF 71 A75039, 1975.

7. LANGEN, I.: FEDA, A General Dynamic Analysis Program for Linear Structures, User's Manual, SINTEF Report STF 71 A77001, 1977.

8. VUGTS, J.H.: "The Hydrodynamic Coefficients for Swaying, Heaving and Rolling Cylinders in a Free Surface", Int. Shipbuilding Progr., Vol. 15, pp. 251-276, 1968.

9. VUGTS, J.H.: "The Hydrodynamic Forces and Ship Motions in Waves", Dr. Thesis, Delft, 1970.

10. FRANK, W.: Oscillation of Cylinders in or below the Free Surface of Deep Fluids, Naval Ship Research and Development Center, Washington DC, Report No. 2375, 1967.

11. FALTINSEN, O.: A Comparison of Frank Close-Fit Method with some other Methods used to find Two-dimensional Hydro-dynamic Forces and Moments for Bodies which are Oscillating Harmonically in an Ideal Fluid, Report No. 69-43-3. Det norske Veritas, Nov. 1969.

12. WEHAUSEN, J.V.: The Motion of Floating Bodies, Rev. Fluid Mech., Vol. 3, 1971.

13. Flytebro over Salhusfjorden: To-dimensjonale forsøk, Delrapport no. 1, River and Harbour Laboratory at the Norwegian Institute of Technology, Trondheim, Nov. 1968.

14. KINSMAN, B.: Wind Waves, Prentice Hall, 1965.

15. GOTO, H. and TOKI, K.: Structural response to nonstationary random exitation, Proc. of the Fourth World Conference on Earthquake Engineering, Santiago, Chile, 1969.

16. SHINOZUKA, M.: Simulation of Multivariate and Multidimensional Random Process, The Journal of the Acoustical Society of America, Vol. 49, 1971.

17. SHINOZUKA, M.: Monte Carlo Solution of Structural Dynamics, Computers and Structures, Vol. 2, 1972.

18. HOUMB, O.G.: Flytebro over Salhusfjorden: Bølgeanalyse, Delrapport nr. 3, River and Harbour Laboratory at the Norwegian Institute of Technology, Trondheim, Oct. 1969.

19. HASSELMANN, K. et al.: Measurements of Wind-Wave Growth and Swell Decay during the Joint North Sea Wave Project (JONSWAP), Ergänzungsheft zur Deutschen Hydrographischen Zeitschrift, Reihe A (8°), Nr. 12, 1973.

20. CARTWRIGHT, D.E. and LONGUET-HIGGINS, M.S.: The Statistical Distribution of the Maxima of a Random Function, Proceedings of the Royal Society of London, Series A, Vol. 237, Oct. 1956.